Effect of Process Variation on Field Emission Characteristics in Surface-Conduction Electron Emitters

Hsiang-Yu Lo, Yiming Li, *Member, IEEE*, Chih-Hao Tsai, Hsueh-Yung (Robert) Chao, and Fu-Ming Pan

***Abstract*—In this paper, we explore the effect of process variation on field emission characteristics in surface-conduction electron emitters. The structure of Pd thin-film emitter is fabricated on the substrate and the nanometer scale gap is formed by the focused ion beam technique. Different shapes of nanogaps due to the process variations are investigated by the experiment and three-dimensional Maxwell particle-in-cell simulation. Four deformation structures are examined, and it is found that the type 1 exhibits high emission efficiency due to a stronger electric field around the apex and larger emission current among structures. The electron emission current is dependent upon the angle of inclination of surface. Hydrogen plasma treatment is also used to increase the edge roughness of the nanogap and thereby dramatically improve the field emission characteristics. For the nanogap with a separation of 90 nm, the turn-on voltage significantly reduces from 60 to 20 V after the hydrogen plasma treatment.**

***Index Terms*—Angle of inclination of surface, field emission, hydrogen plasma, Maxwell equations, nanogap, Pd, particle-in-cell (PIC) simulation, process variations, shape, surface-conduction electron emitters (SCEs), thin-film emitter, turn-on voltage.**

I. Introduction

APPLICATIONS of electrodes with nanometer separation have recently been of great interest in molecular electronics [1], [2], biosensors [3], and vacuum microelectronics [4]. However, known researches of nanogap are only in their infancy because complicated fabrication processes cannot be modeled well. One of up-to-date applications of nanogap is the surface-conduction electron emitter (SCE) for the flat panel displays (FPDs). The surface-conduction electron-emitter display (SED) is a new type of FPD based upon SCEs [5]–[7]. SEDs possess high luminance, wide viewing angle, quick response time, and low power consumption, compared with other FPDs such as liquid crystal displays and plasma display panels. The critical process step to fabricate an SCE is to create a nanofissure on a line electrode where the electron emission occurs. It results in rather complicated and expensive procedure in the nanogap fabrication technique. The field emission characteristics of SED devices are seriously affected by the material and geometric parameters, the separation of nanogaps, and the morphology of edge surface of the emitters. Unfortunately, computer simulation of SCE has not been clearly drawn yet. As a result, a study of obtaining high emission current, high emission efficiency, and stable fabrication of nanogap becomes one of interesting issues.

In this paper, we explore the field emission properties of four deformed Pd nanogaps that are fabricated by the focused ion beam (FIB) technique [8]. This fabrication approach is simple and well controlled. We use a calibration model for analyzing the field emission efficiency of the structure of Pd thin-film emitter with nanogap of 90 nm under different conditions. A particle-in-cell (PIC) numerical simulation is further performed in this study. We consider a 3-D finite-difference time-domain (FDTD) method for self-consistent simulation of the electromagnetic fields and charged particles. It enables us to explore electron emission properties with one Pd electron emitter. In the field emission process, electron emission is modeled by the Fowler–Nordheim (F-N) equation [9], where the conducting mechanism of the device could be explained. Furthermore, in order to improve the emission current of the nanogap, we have performed surface modification for the Pd electrodes with hydrogen plasma treatment. It enhances the surface roughness of the nanogaps and generates higher electric fields for the electron emission.

The experimental procedures of fabricating the nanogap are presented, and then, we introduce the four types of deformation in Section II. We briefly state the solution methods in Section III. The emission *I–V* characteristics, the electronic trajectories, and the field distribution near the nanogaps are examined in Section IV. The high field emission efficiency after hydrogen plasma treatment is also analyzed experimentally in this section. Finally, we conclude that different process variations lead to varied emission current.

II. Fabrication Procedure

Fig. 1 schematically shows the structure of the SCE device. P-type (1 0 0) Si wafer is used as the substrate. A 150-nm-thick SiO_2 layer is first thermally grown on the Si substrate. The Ti layer with 5 nm thick is electron-beam-evaporation (e-beam) deposited on the oxide as an adhesion layer for the subsequently

Manuscript received July 5, 2007; revised November 23, 2007. This work was supported in part by the Taiwan National Science Council (NSC) under Contract NSC-96-2221-E-009-210 and Contract NSC-96-2752-E-009-003-PAE, in part by the Ministry of Education (MoE) Aim for Top University (ATU) Project, Taiwan, R.O.C., under Grant 2006-2007, and in part by the Chunghwa Picture Tubes under Grant 2006-2008. The review of this paper was arranged by Associate Editor R. Lake.

H.-Y. Lo and Y. Li are with the Department of Communication Engineering, National Chiao Tung University, Hsinchu 300, Taiwan, R.O.C. (e-mail: ymli@faculty.nctu.edu.tw).

C.-H. Tsai and F.-M. Pan are with the Department of Materials Science and Engineering, National Chiao Tung University, Hsinchu 300, Taiwan, R.O.C.

H.-Y. Chao is with Physware, Inc., Bellevue, WA 98004 USA.

Color versions of one or more of the figures in this paper are available online at http://ieeexplore.ieee.org.

Digital Object Identifier 10.1109/TNANO.2008.926347

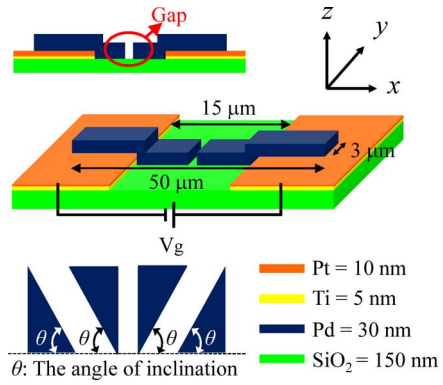

Fig. 1. Schematic plot of SCE structure and cross section of SCE in x–z plane. The thicknesses of this device are shown in the bottom-right corner.

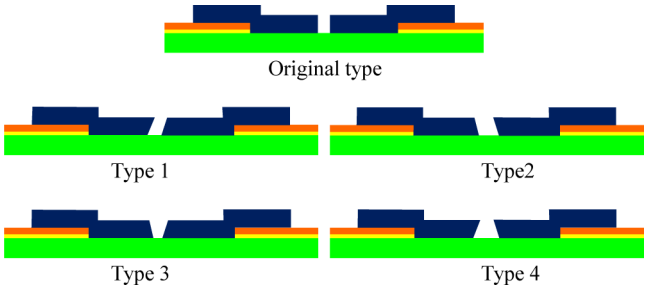

Fig. 2. Cross-sectional plots along the x–z plane. Four types of the SCEs caused by process variation are considered in this study. The first plot shows the normal one of the SCE.

e-beam deposited Pt thin film with a thickness of 10 nm. Pattering of the Pt/Ti line electrodes with a width of 80 μm is photolithographically performed using liftoff method. The Pd thin film 30 nm thick is then e-beam deposited on the Pt/Ti bottom electrode and the liftoff method is also used to pattern the Pd electrode line 50 μm long and 3 μm wide. A nanogap with a separation of 90 nm on the Pd strip is then produced by the FIB. Electron emission characteristics in the nanogap are studied using a dc voltage power supply. The measurement is carried out under a vacuum condition of 1.0×10^{-6} torr. This fabrication method is easily reproducible and compatible with contemporary IC technology. The width of nanogap of original type can be readily controlled by tuning the ion beam energy. However, the four types of nanogaps, shown in Fig. 2, could be induced by the process variations in FIB operations or predefined by other fabrication methods [10], [11].

A planar view of SEM image of the original type is shown in Fig. 3. The edges of emitter are smooth and straight according to the SEM observation. The type 1 may be formed by adjusting the direction of FIB with a proper angle. Type 2 is the inverse of type 1 by changing the opposite direction of the FIB in type 1. Type 3 can be fabricated by using advanced microfabrication technology based on FIB, dry etching, and thermal oxidation [10]. Type 4 is found in [11] by using the same technique FIB. To verify the surface-conducting characteristics, effects on the process variation are examined. The increased emission

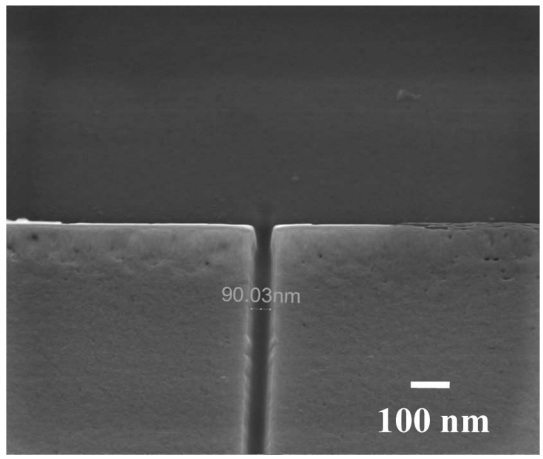

Fig. 3. SEM image of the nanogap formed on the Pd strip in the SCE structure by using FIB technique. The scale bar indicates a length of 100 nm.

current and high emission efficiency after the hydrogen plasma treatment will be shown in Section IV.

III. Method of Calculation

We first formulate a calibration model with the experimental data by using the simulation program that has been developed to calculate the emission efficiency of different SCEs. The electromagnetic PIC codes are performed in the numerical simulation, where the computational flowchart is shown in Fig. 4.

Starting from a specified initial state, we simulate electrostatic fields as its evolution in time. We then perform a time integration of Faraday's law, Ampere's law, and the relativistic Lorentz equation [12], [13]

$$\begin{cases} \dfrac{\partial \mathbf{B}}{\partial t} = -\nabla \times \mathbf{E} \\ \dfrac{\partial \mathbf{E}}{\partial t} = -\dfrac{\mathbf{J}}{\varepsilon} + \dfrac{1}{\mu\varepsilon}\nabla \times \mathbf{B} \\ \mathbf{F} = q\left(\mathbf{E} + \mathbf{v} \times \mathbf{B}\right) \qquad \text{and} \qquad \dfrac{\partial \mathbf{x}}{\partial t} = \mathbf{v} \end{cases} \tag{1}$$

subject to constraints provided by Gauss's law and the rule of divergence of $\mathbf{B}$

$$\nabla \cdot \mathbf{E} = \frac{\rho}{\varepsilon} \text{ and } \nabla \cdot \mathbf{B} = 0. \tag{2}$$

We notice that $\mathbf{E}$ and $\mathbf{B}$ are the electric and magnetic fields, $\mathbf{x}$ is the position of charge particle, and $\mathbf{J}$ and ρ are the current density and charge density resulting from charge particles. The full set of Maxwell's time-dependent equations is simultaneously solved to obtain electromagnetic fields. Similarly, the Lorentz force equation is solved to obtain relativistic particle trajectories. In addition, the electromagnetic fields are advanced in time at each time step. The charged particles are moved according to the Lorentz equation using the fields advanced in each time step. The weighted charge density and current density at the grids are subsequently calculated. The obtained charge density and current density are successively used as sources in the 3-D Maxwell equations for advancing the electromagnetic fields. These steps are repeated for each time step until the specified

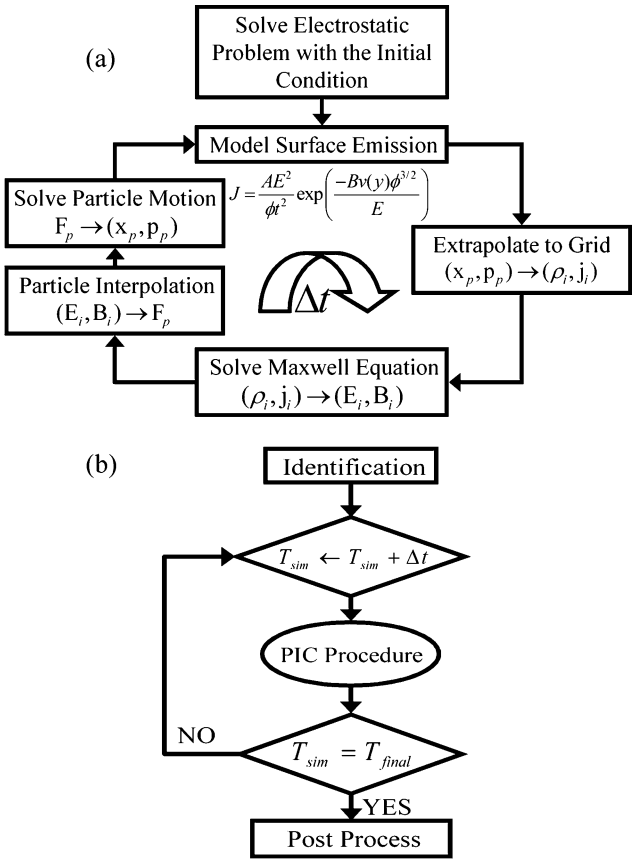

Fig. 4. (a) Flowchart of the PIC procedure. (b) Computational scheme for the simulation, where the block of the PIC procedure is shown in (a).

number of time steps is reached. We notice that the space–charge effects are automatically included in the simulation algorithms. The effect of space–charge on field emission was discussed by Stern *et al.* [14]. This 3-D FDTD-PIC method thus approaches to self-consistent simulation of the electromagnetic fields and charged particles.

In the field emission process, the electron emission is modeled by the F-N equation [8]

$$J = \frac{AE^2}{\varphi t^2}\exp\left(\frac{-Bv\,(y)\,\varphi^{3/2}}{E}\right) \tag{3}$$

where $A = 1.541 \times 10^{-6}\text{A}\cdot\text{eV}/\text{V}^2$ and $B = 6.3408 \times 10^8\ \text{eV}^{-3/2}\cdot\text{V}\cdot\mu\text{m}^{-1}$, E is the normal component of the electric field at the emitter surface, φ is the work function of the emission material, t^2 is approximately equal to 1.1, and $v(y) = 0.95 - y^2$, with $y = 3.79 \times 10^{-5} \times E^{1/2}/\varphi$ being in SI unit. The emission current density is determined by (3) according to the local electric field, the work function of emitter material, and the geometric factors. We notice that, in the entire simulation, all dimensions of physical quantities are the same with the experimental settings.

IV. Results and Discussion

For exploring the effects of the gate voltages and the inclined angle of nanogaps upon the emission current, we analyze the electron trajectories and the electric fields simultaneously. For

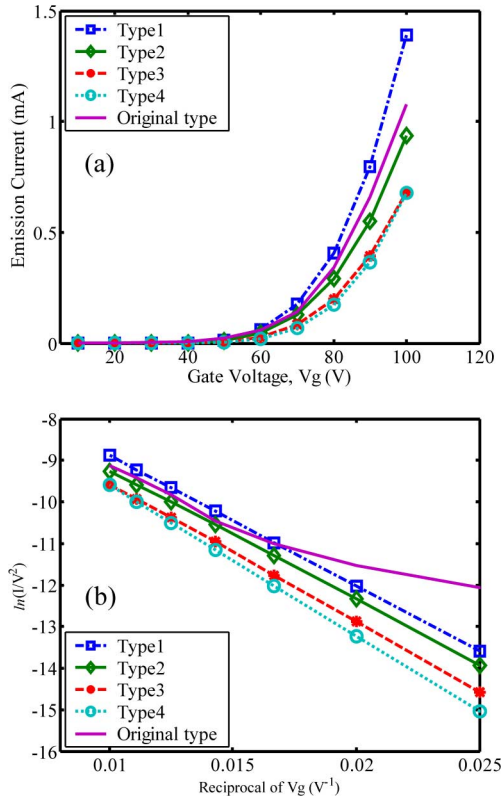

Fig. 5. (a) *I–V* characteristics of the SCE device with different types caused by process variations. (b) Corresponding F-N plot indicating the true nature of field emission.

the constant angle of inclination, the computed *I–V* characteristics with various nanogap emitters compared with the experimental data of the nanogap of original type are shown in Fig. 5. When the gate voltage varies from 10 to 100 V, the four kinds of symbols indicate the simulated data of four types and the line represents the experimental data of original type. It is found, shown in Fig. 5(a), that the turn-on voltage of 60 V is obtained at an emission current of 70 μA for nanogap of 90 nm wide. However, there is a significant effect upon the electron emission of the inclination of surface and gate voltage. When the gate voltage is 60 V, we find that the emission current of type 1 and type 2 are larger than the emission current of the original type, but as the gate voltage is raised to 100 V, only the emission current of type 1 is larger than the emission current of the original type. A very high emission current of 0.3 mA is estimated at the gate voltage of 80 V for the emitter of 90 nm wide. The corresponding F-N plot [i.e., a plot between $\ln(I/V^2)$ and $1/V$] of the field emission of Pd SCE is shown in Fig. 5(b). Assuming the work function $\varphi = 5.12$ eV for Pd, the linear relationships in the high-voltage region indicate that the electron conduction followed the F-N field emission mechanism.

When the gate voltage is fixed at 60 V and the inclined angle is 60°, the electric field contours with different types of nanogaps are shown in Fig. 6. The local electric field near the nanogap, shown in Fig. 6(b), is higher than Fig. 6(a) and (c)–(e). Therefore, the emission current in Fig. 6(b) should be higher than that of Fig. 6(a) and (c)–(e). This structure of type 1 that has a tip around the corner on the left electrode implies that it can

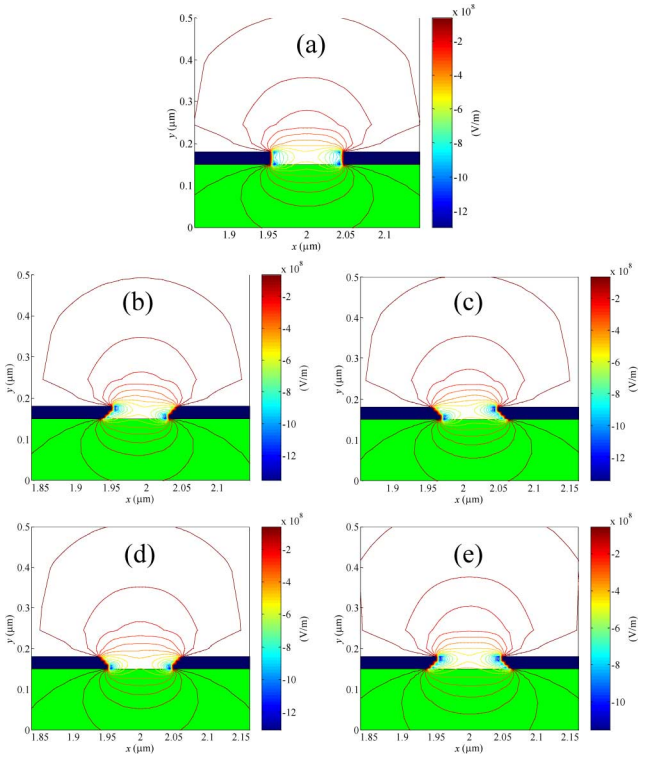

Fig. 6. Contour plots of electric fields. (a) Original type. (b) Type 1. (c) Type 2. (d) Type 3. (e) Type 4. The width of nanogap is approximately 90 nm, the angle of inclination is 60°, and the gate voltage is 60 V.

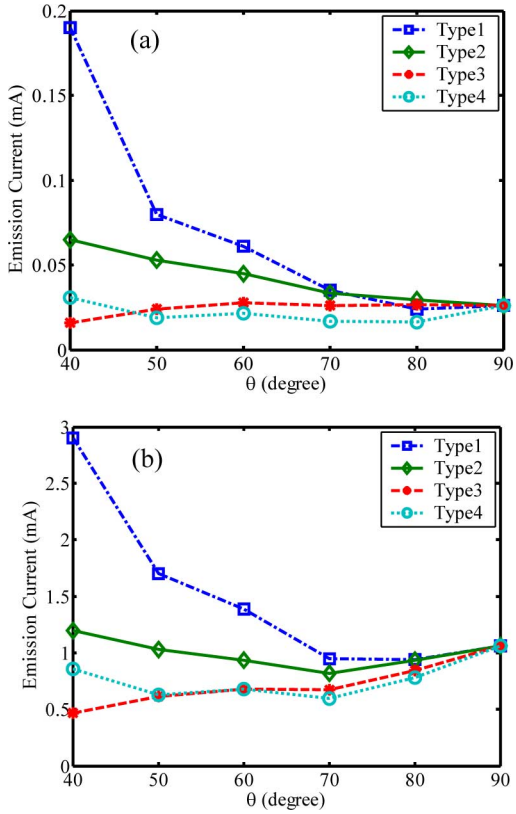

Fig. 7. Plot of the inclined angles of surface versus the emission current, where the width of nanogap is 90 nm. The gate voltage is (a) 60 V and (b) 100 V, respectively.

produce high electric fields around the emitter apex, and generate high emission current.

Fig. 7 compares the electron emission current with angle of inclination under two different gate voltages. We find that the emission current attains the maximum in the type 1 and it is always larger than the value when the surface is vertical (the same fact as shown in Fig. 5). When the angle is smaller than 90°, the emission efficiency has no improvement in the type 3 and type 4. This phenomenon is caused by the electric fields are not concentrated on the emitted surface and the distributed electric field broadens the potential barrier at the metal–vacuum interface for the electrons to have a less chance of tunneling from the solid into vacuum. It is obvious that the type 3 and type 4 are not seriously influenced by the inclination of surface, but the type 1 can improve the emission efficiency when the angle is smaller. In addition, decreasing the inclined angle or the gate voltage can enhance the emission current in type 2.

High brightness and long lifetime are the main targets of emission material investigations for scientific instrument applications, but high current density and low power consumption are the guiding rules for display applications. Hence, we here explored the emission characteristics caused by different material work functions with respect to the nanogap of original type because changes of the local work functions lead to field emission current fluctuation [15]. Therefore, we propose that the morphology of nanogap edge can be greatly modified by the plasma treatment. After a hydrogen plasma treatment on the SCE device, the edges become very rough due to severe ion bombardment. The surface-conducting properties of the SCE can be great of progress after the hydrogen plasma treatment. Fig. 8(a) shows the field emission *I–V* curves for the Pd emitter with a 90 nm nanogap after the plasma treatment under various treatment times and the corresponding F-N plot is shown in Fig. 8(b). We can find the emission current increase after this treatment. Here, the turn-on voltage is defined as the gate voltage at which the F-N plot began to show the linear behavior, as marked by circle in Fig. 8(b). In addition, the zoom-in plot of red line that can be clearer to know the electron emission mechanism is shown in the upper plot of Fig. 8(b). We can find that the turn-on voltages near 80 and 70 V are observed in the 90 nm nanogap with no hydrogen plasma treatment and hydrogen plasma treatment for 1 min, respectively. After the hydrogen plasma treatment for 3 min, the turn-on voltage dropped from 80 to 30 V. From the observations of Fig. 8, the emission current indeed convinces the mechanism of F-N model. The significant reduction in the turn-on voltage after the hydrogen plasma treatment might be ascribed to the formation of a rugged nanogap edge and the decrease of the work function in the electron-emitting area. During the hydrogen plasma treatment, the Pd electrodes are subject to hydrogen ion bombardment leading to the formation of a rough surface on the Pd electrodes. The nanogap edges thus become rugged as well according to the SEM study, which is shown in Fig. 9. Therefore, electric fields can concentrate around areas with sharp features resulting in the enhancement of field emission efficiency [10]. In addition, the surfaces of Pd electrodes are hydrogenated during the plasma treatment forming

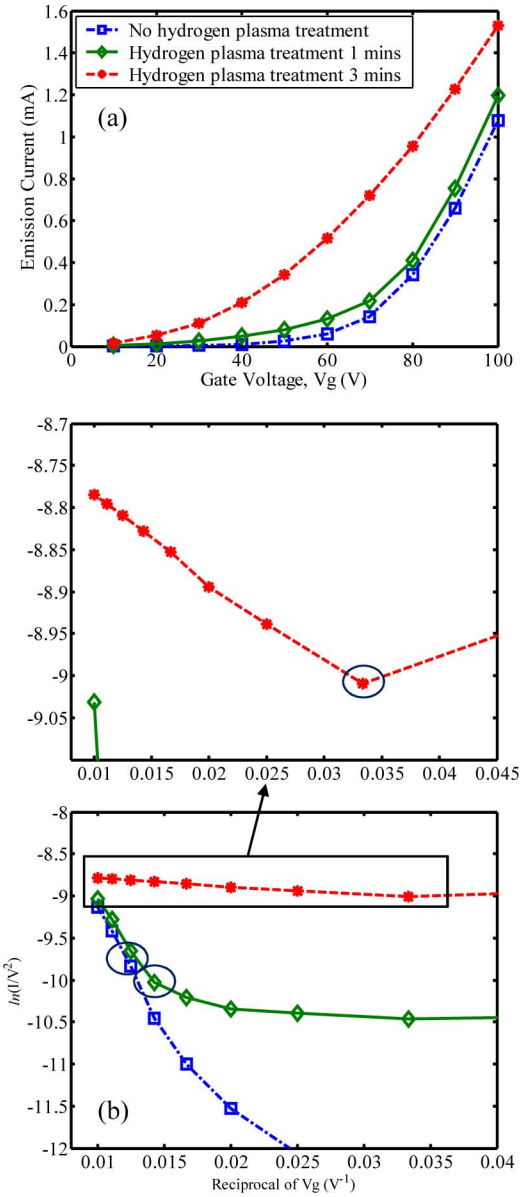

Fig. 8. (a) Field emission *I–V* characteristics for the nanogap of 90 nm wide after the hydrogen plasma treatment under various treatment times. (b) Corresponding F-N plot of (a) and the zoom-in plot of red line.

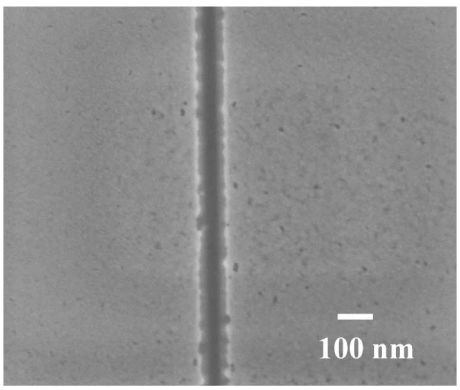

Fig. 9. SEM image of the nanogap formed on the Pd strip after 3 min of hydrogen plasma treatment. The scale bar indicates a length of 100 nm.

Pd hydrides that have a smaller work function than the metallic Pd [16]. The reduction in the work function of the emitter surface can effectively increase the field emission current and thereby decrease the turn-on voltage. Except the process variations on nanogap, controlling the roughness and the local work function at emission point are also important issues.

V. Conclusion

We have successfully fabricated nanogap with a separation of 90 nm on the Pd electrode in the SED emitter structure using FIB technique. The width of nanogap can be readily controlled by tuning the ion beam energy and it also easily leads to the process variations. To verify the emission characteristics, effects on the process variation have been examined. Our results imply that the decrease in the angle of inclination of surface is effective but may not suit all cases except the type 1. One of the best choices of the shape under the conditions of process variation is the type 1 due to its stronger electric field around the apex and larger emission current. Hydrogen plasma treatments could greatly reduce the turn-on voltage. The turn-on voltage of the 90 nm Pd nanogap can be reduced from 80 to 30 V after the hydrogen plasma treatment for 3 min. The decrease is ascribed to the formation of a rugged nanogap edge and surface Pd hydrides.

References

[1] M. A. Reed, C. Zhou, C. J. Muller, T. P. Burgin, and J. M. Tour, "Conductance of a molecular junction," *Science*, vol. 278, no. 5336, pp. 252–254, Oct. 1997.

[2] Bezryadin and C. Dekker, "Nanofabrication of electrodes with sub-5 nm spacing for transport experiments on single molecules and metal clusters," *J. Vac. Sci. Technol. B*, vol. 15, no. 4, pp. 793–799, Jul. 1997.

[3] S. Oh, J. S. Lee, K. H. Jeong, and L. P. Lee, "Minimization of electrode polarization effect by nanogap electrodes for biosensor applications," in *Proc. IEEE MEMS,* Jan. 2003, pp. 52–55.

[4] H. I. Lee, S. S. Park, D. I. Park, S. H. Ham, J. H. Lee, and J. H. Lee, "Nanometer-scaled gap control for low voltage and high current operation of field emission array," *J. Vac. Sci. Technol. B*, vol. 16, no. 2, pp. 762–764, Mar. 1998.

[5] Nomura , K. Sakai, E. Yamaguchi, M. Yamanobe, S. Ikeda, T. Hara, K. Hatanaka, and Y. Osada, "A new emissive display based on surface-conduction electron-emitters," in *Proc. IDW*, 1996, pp. 523–526.

[6] K. Sakai, I. Nomura, E. Yamaguchi, M. Yamanobe, S. Ikeda, T. Hara, K. Hatanaka, Y. Osada, H. Yamamoto, and T. Nakagiri, "Flat-panel displays based on surface-conduction electron-emitters," in *Proc. EuroDisplay,* 1996, pp. 569–572.

[7] E. Yamaguchi, K. Sakai, I. Nomura, T. Ono, M. Yamanobe, N. Abe, T. Hara, K. Hatanaka, Y. Osada, H. Yamamoto, and T. Nakagiri, "A 10-in. surface-conduction electron-emitter display," *J. Soc. Inf. Display*, vol. 5, no. 4, pp. 345–348, 1997.

[8] Y. Goth, T. Ohtake, N. Fujita, K. Inoue, H. Tsuji, and J. Ishikawa, "Fabrication of lateral-type thin-film edge field emitters by focus ion beam technique," *J. Vac. Sci. Technol. B*, vol. 13, no. 2, pp. 465–468, 1995.

[9] R. H. Fowler and L. W. Nordheim, "Electron emission in intense electric fields," *Proc. R. Soc. Land. A*, vol. 119, no. 781, pp. 173–181, May 1928.

[10] H. Fujii, S. Kanemaru, H. Hiroshima, S. M. Gorwadkar, T. Matsukawa, and J. Itoh, "Fabrication and characterization of a nanogap edge emitter with a silicon-on-insulator wafer," *Appl. Surf. Sci.*, vol. 146, no. 1, pp. 203–208, 1999.

[11] K. Shigeto, M. Kawamura, A. Yu. Kasumov, K. Tsukagoshi, K. Kono, and Y. Aoyagi, "Reproducible formation of nanoscale-gap electrodes for single-molecule measurements by combination of FIB deposition and tunneling current detection," *Microelectron. Eng.*, vol. 83, no. 4, pp. 1471–1473, Apr. 2006.

[12] C. K. Birdsall and A. B. Langdon, *Plasma Physics via Computer Simulation*. New York: McGraw-Hill, 1985.

[13] B. Goplen, L. Ludeking, D. Smithe, and G. Warren, "User-configurable MAGIC for electromagnetic PIC simulation," *Comput. Phys. Commun.*, vol. 87, pp. 54–86, Jan. 1995.
[14] T. E. Stern, B. S. Gosling, and R. H. Fowler, "Further studies in the emission of electrons from cold metals," *Proc. R. Soc. Land. A*, vol. 124, no. 795, pp. 699–723, Jul. 1929.
[15] S. Yamamoto, "Fundamental physics of vacuum electron sources," *Rep. Prog. Phys.*, vol. 69, no. 1, pp. 181–232, Jan. 2006.
[16] R. Dus, R. Nowakowski, and E. Nowicka, "Chemical and structural components of work function changes in the process of palladium hydride formation within thin Pd film," *J. Alloy Compd.*, vol. 404–406, pp. 284–287, Dec. 2005.

Hsiang-Yu Lo was born on December 22, 1983, in Taiwan. He received the B.S. degree from the Department of Electrophysics, National Chiao Tung University, Hsinchu, Taiwan, R.O.C., in 2006, and the M.S. degree from the Department of Communication Engineering, National Chiao Tung University, in 2007.

His research interests include computational electronics and simulation of surface-conduction electron emission for display technology.

Yiming Li (M'02) received the B.S. degree in applied mathematics and electronics engineering, the M.S. degree in applied mathematics, and the Ph.D. degree in electronics from the National Chiao Tung University (NCTU), Hsinchu, Taiwan, R.O.C., in 1996, 1998, and 2001, respectively.

In 2001, he joined the National Nano Device Laboratories (NDL), Taiwan, as an Associate Researcher, where, from 2003 to 2005, he was the Director of the Departments of Nanodevice and Computational Nanoelectronics. He was an Assistant Professor at the Microelectronics and Information Systems Research Center (MISRC), National Chiao Tung University (NCTU), where he became an Associate Professor in the fall of 2004, and is currently an Associate Professor in the Department of Communication Engineering, an Adjunct Professor at the Institute of Management of Technology, the Deputy Director of the Modeling and Simulation Center, and also conducts the Parallel and Scientific Computing Laboratory. He has been engaged in the field of computational science and engineering, particularly in modeling, simulation, and optimization of nanoelectronics and very large scale integration (VLSI) circuits. In the fall of 2002, he was a Visiting Assistant Professor in the Department of Electrical and Computer Engineering, University of Massachusetts at Amherst. From 2003 to 2004, he was a Research Consultant of the System on a Chip (SOC) Technology Center, Industrial Technology Research Institute (ITRI), Hsinchu. His current research interests include computational electronics and physics, physics of semiconductor nanostructures, device modeling, parameter extraction, and VLSI circuit simulation, development of technology computer-aided design (TCAD) and electronic CAD (ECAD) tools and SOC applications, bioinformatics and computational biology, and advanced numerical methods, parallel and scientific computing, optimization techniques, and computational intelligence. He has authored or coauthored over 120 research papers appearing in international book chapters, journals, and conferences. He has served as a reviewer, Guest Associate Editor, and Guest Editor for many international journals.

Dr. Li has organized and served on several international conferences and was an editor for proceedings of international conferences. He is a member of Phi Tau Phi, Sigma Xi, the American Physical Society, the American Chemical Society, the Association for Computing Machinery, the Institute of Electronics, Information and Communication Engineers (IEICE), Japan, and the Society for Industrial and Applied Mathematics. He is included in *Who's Who in the World*. He has been a reviewer for the IEEE TRANSACTIONS ON NANOTECHNOLOGY, the IEEE TRANSACTIONS ON EVOLUTIONARY COMPUTATION, the IEEE TRANSACTIONS ON MICROWAVE THEORY AND TECHNIQUES, the IEEE TRANSACTIONS ON COMPUTER-AIDED DESIGN OF INTEGRATED CIRCUITS AND SYSTEMS, the IEEE ELECTRON DEVICE LETTERS, and the IEEE TRANSACTIONS ON ELECTRON DEVICES. He was the recipient of the 2002 Research Fellowship Award presented by the Pan Wen-Yuan Foundation, Taiwan, and the 2006 Outstanding Young Electrical Engineer Award from the Chinese Institute of Electrical Engineering, Taiwan.

Chih-Hao Tsai was born in Taichung, Taiwan, R.O.C., in 1978. He received the B.S. and M.S. degrees in materials science and engineering from the Feng Chia University, Taichung, in 2002 and 2004, respectively. He is currently working toward the Ph. D. degree at the Department of Materials Science and Engineering, National Chiao Tung University, Hsinchu, Taiwan.

His current research interests include all solid-state thin-film batteries, electromechanical properties of nanostructured materials, and novel devices for field emission display.

Hsueh-Yung (Robert) Chao was born on January 7, 1973, in Taiwan, R.O.C. He received the B.S. degree from the National Sun Yat-Sen University, Kaohsiung, Taiwan, in 1994, and the M.S. and Ph.D. degrees from the University of Illinois at Urbana-Champaign, Urbana-Champaign, in 1998 and 2002, respectively.

From 1996 to 2002, he was a Research Assistant at the Center for Computational Electromagnetics, University of Illinois at Urbana-Champaign. In 1999 and 2002, he held summer internships with Intel Corporation, Hillsboro, OR, where in 2003, he was a Senior CAD Engineer in the Technology Computer-Aided Design (CAD) Department. In 2004, he was an Assistant Professor in the Department of Communication Engineering, National Chiao Tung University, Taiwan. Since 2008, he has been the Research and Development Manager at Physware, Inc., Bellevue, WA. His current research interests include fast algorithms for computational electromagnetics, simulation of plasma physics, optical imagining in microlithography, adaptive mesh generation, circuit synthesis, and numerical analysis.

Fu-Ming Pan received the Ph.D. degree in physical chemistry from the University of California, Irvine, in 1984.

He was a Postdoctoral Researcher in the Department of Chemistry, Northwestern University, for two years. Until 1993, he was with the Materials Characterization Group, Materials Research Laboratory, Industrial Technology Research Institute (ITRI), Taiwan. Till 2003, he was with the National Device Laboratories. He is currently a Professor in the Department of Materials Science and Engineering, National Chiao Tung University, Hsinchu, Taiwan. His current research interests include fabrication of nanostructured materials for field emission applications and Cu interconnect technology.